Eur. J. Biochem. **271**, 2280–2290 (2004) © FEBS 2004 doi:10.1111/j.1432-1033.2004.04173.x

Binding of the potential antitumour agent indirubin-5-sulphonate at the inhibitor site of rabbit muscle glycogen phosphorylase b

Comparison with ligand binding to pCDK2–cyclin A complex

Magda N. Kosmopoulou[1], Demetres D. Leonidas[1], Evangelia D. Chrysina[1], Nicolas Bischler[1], Gerhard Eisenbrand[3], Constantinos E. Sakarellos[4], Richard Pauptit[5] and Nikos G. Oikonomakos[1,2]

[1]*Institute of Organic and Pharmaceutical Chemistry, and* [2]*Institute of Biological Research and Biotechnology, The National Hellenic Research Foundation, Athens, Greece;* [3]*Department of Chemistry, Division of Food Chemistry and Environmental Toxicology, University of Kaiserslautern, Germany;* [4]*Department of Chemistry, University of Ioannina, Greece;* [5]*AstraZeneca, Macclesfield, UK*

The binding of indirubin-5-sulphonate (E226), a potential anti-tumour agent and a potent inhibitor (IC_{50} = 35 nM) of cyclin-dependent kinase 2 (CDK2) and glycogen phosphorylase (GP) has been studied by kinetic and crystallographic methods. Kinetic analysis revealed that E226 is a moderate inhibitor of GPb (K_i = 13.8 ± 0.2 μM) and GPa (K_i = 57.8 ± 7.1 μM) and acts synergistically with glucose. To explore the molecular basis of E226 binding we have determined the crystal structure of the GPb/E226 complex at 2.3 Å resolution. Structure analysis shows clearly that E226 binds at the purine inhibitor site, where caffeine and flavopiridol also bind [Oikonomakos, N.G., Schnier, J.B., Zographos, S.E., Skamnaki, V.T., Tsitsanou, K.E. & Johnson, L.N. (2000) *J. Biol. Chem.* **275**, 34566–34573], by intercalating between the two aromatic rings of Phe285 and Tyr613. The mode of binding of E226 to GPb is similar, but not identical, to that of caffeine and flavopiridol. Comparative structural analyses of the GPb–E226, GPb–caffeine and GPb–flavopiridol complex structures reveal the structural basis of the differences in the potencies of the three inhibitors and indicate binding residues in the inhibitor site that can be exploited to obtain more potent inhibitors. Structural comparison of the GPb–E226 complex structure with the active pCDK2–cyclin A–E226 complex structure clearly shows the different binding modes of the ligand to GPb and CDK2; the more extensive interactions of E226 with the active site of CDK2 may explain its higher affinity towards the latter enzyme.

Keywords: indirubin-5-sulphonate; inhibitor; glycogen phosphorylase; type 2 diabetes; X-ray crystallography.

Inhibitors of glycogen phosphorylase (EC 2.4.1.1; GP) have been proposed as a therapeutic strategy for improving glycaemic control in type 2 diabetes mellitus and various studies have shown the efficacy of such compounds at lowering blood glucose or inhibiting liver glycogenolysis *in vivo* [1–3]. GP is an allosteric enzyme that exists in two interconvertible forms, GPb (low activity, predominantly T state) and GPa (high activity, predominantly R state) [4,5]. GPa plays a major role in the regulation of glycogen degradation [6–8] as well as in proliferating cells [9]. Previous studies have shown that flavopiridol, a compound with promising anti-tumour properties, that targets cyclin-dependent kinases (CDKs) 1,2,4,7 by binding to the ATP binding site [10], was also inhibiting the activity of GP [11]. Flavopiridol binds at the inhibitor site of GP [12], a highly hydrophobic binding pocket, located 12 Å from the catalytic site. Compounds such as flavopiridol, which target both CDK2 and GP, could have a combined action in tumour cells by disrupting the cell cycle and sending cells to apoptosis while starving cancer cells of glucose.

It has been reported that indirubins are potent inhibitors of CDKs [50% inhibitory concentrations (IC_{50}) in the 50–100 nM range], a family of key cell cycle regulators [13]. One of these, indirubin-5-sulphonate (E226) (Scheme 1) was found to be a potent competitive inhibitor (with respect to ATP) of monomeric CDK2 (IC_{50} = 35 nM) [13] and pCDK2–cyclin A complex [14]. Indirubins have also been shown to be potent inhibitors of glycogen synthase kinase-3β (GSK-3β), an enzyme that has been implicated in Alzheimer′ disease, type 2 diabetes and cancer [15]. Indirubin-3′-monoxime is extremely potent (IC_{50} = 22 nM) and E226 is less potent (IC_{50} = 280 nM) against GSK-3β. Recently, the discovery of new classes of 6-substituted and 5,6-disubstituted indirubins as potent inhibitors of GSK-3 was reported [16,17]. The effect of indirubins on GSK-3 might contribute to a potential antidiabetic action of these

Correspondence to N. G. Oikonomakos, Institute of Organic & Pharmaceutical Chemistry, The National Hellenic Research Foundation, 48 Vas. Constantinou Ave., 11635 Athens, Greece. Fax: + 30 210 7273831, Tel.: + 30 210 7273761, E-mail: ngo@eie.gr

Abbreviations: CDK, cyclin-dependent kinase; pCDK2/cyclin A, Thr160 phosphorylated cyclin-dependent kinase 2-cyclin complex; E226, indirubin-5-sulphonate; Glc1-P, α-D-glucose 1-phosphate; glucose, α-D-glucose; GP, glycogen phosphorylase; GPa, muscle glycogen phosphorylase a; GPb, muscle glycogen phosphorylase b; IMP, inosine 5′-monophosphate; PLP, pyridoxal 5′-phosphate.

Enzymes: glycogen phosphorylase (EC 2.4.1.1).

(Received 22 January 2004, revised 16 March 2004, accepted 19 April 2004)

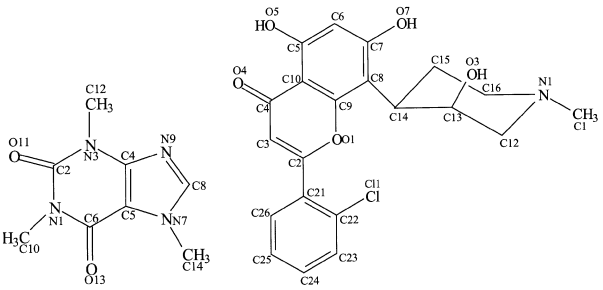

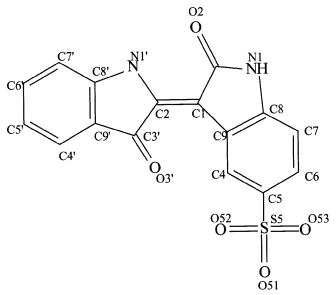

Scheme 1. The chemical structures of caffeine, flavopiridol and E226 (showing the numbering system used).

compounds and thus enhance the effects mediated by inhibition of GP.

In this work we investigated whether E226 inhibits GP activity. Kinetic studies have revealed that E226 inhibits both muscle GPb and GPa and mimics the inhibition of caffeine and flavopiridol. In order to provide a stereochemical explanation for E226 inhibition, we have determined the structure of GPb–E226 at 2.3 Å resolution. The results show that E226 binds at the inhibitor site. Comparison of the structure of the GPb–E226 complex with the structures of GPb–caffeine and GPb–flavopiridol complexes provides useful information for the design of new potent inhibitors of the enzyme. A comparison of the binding of E226 to both GP and pCDK2–cyclin A complex is also presented.

Experimental procedures

Kinetic experiments

Rabbit muscle GPb was isolated, purified, recrystallized, and assayed as described [18]. GPa was prepared and recrystallized as before [19]. Glc1-P (dipotassium salt), AMP, glycogen (oyster) and other chemicals were obtained from Sigma Chemical Company. Glycogen was freed of AMP as described previously [20].

Crystallization and data collection

Native T-state tetragonal ($P4_32_12$) GPb crystals were grown as described previously [12]. Preliminary crystallographic experiments were performed using synchrotron radiation in EMBL-Hamburg, SRS-Daresbury, and X-rays in Jena, by exploring various ligand and dimethyl sulfoxide concentrations. The data for the GPb–E226 complex, presented here, were collected at room temperature at the Center for Design and Structure in Biology, Institute of Molecular Biology, Jena (Germany), using a MAR 345 image plate mounted on a Nonius rotating anode X-ray source with CuKα radiation ($\lambda = 1.5418$ Å) at a maximum resolution of 2.3 Å. A single crystal was soaked in a solution containing 20 mM E226 in 10 mM Bes pH 6.7, 0.1 mM EDTA, 0.02% (w/v) sodium azide, and 20% (v/v) dimethyl sulfoxide for at least 7 h prior to data collection. Crystal orientation and integration of reflections, interframe scaling, partial reflection summation, data reduction and postrefinement were performed using the HKL program suite [21]. Amplitudes were then obtained from the intensities by the TRUNCATE program [22].

Refinement

Crystallographic refinement of the GPb–E226 complex was carried out with CNS version 1.1 [23], using bulk solvent correction. All data were included with no sigma cut-off. The starting model was the refined structure of the GPb–caffeine–IMP complex (Protein Data Bank code 1GFZ [12]) with caffeine removed. Several side chains of the protein residues were adjusted and water molecules were added to the model and retained only if they met stereochemical requirements. Difference electron density maps indicated two possible orientations of E226, related by a rotation of $\approx 180°$ around the short axis of the molecule. Both binding modes were modelled and refined as alternative orientations (I and II) with reduced individual occupancy (0.6 and 0.4, respectively). Apart from sulphonate oxygens, all atoms of E226 were restrained to lie on a single plane. Alternating cycles of manual building with the program O [24], and torsion angle dynamics, conjugate gradient minimization, and restrained individual *B*-factor refinement using the maximum likelihood target function as implemented in CNS were performed until the R_{free} value could not improve any further. A summary of the data processing statistics and refinement parameters is given in Table 1. The program PROCHECK [25] was used to assess the quality of the final structures. The Ramachandran plot [26] showed that all residues lie in the allowed regions.

The structure was analysed with the graphics program O [24]. A model of the inhibitor molecule, E226, was generated using the program SYBYL (Tripos Associates Inc., St Louis, MO, USA) and it was fitted to the sigmaA weighted $2F_o–F_c$ electron density map [27]. Solvent-accessible areas have been calculated for the free and protein-bound inhibitor to provide an estimate of the molecular surface area involved in binding to the enzyme, by using the program NACCESS [28]. Structures were superimposed over well-defined residues using LSQKAB [26]. All figures were prepared with the program MOLSCRIPT [29] and rendered with RASTER3D [30].

Coordinates for the 2.3 Å resolution GPb/E226 complex have been deposited with the RCSB Protein Data Bank (http://www.rcsb.org/) (code 1UZU).

Table 1. Diffraction data and refinement statistics for GPb/E226 complex.

Data collection	
Space group	$P4_32_12$
No. of images ($\Delta\varphi°$)	55 (0.7°)
Unit cell dimensions (Å)	a = b = 128.6, c = 116.4
Resolution range (outermost shell) (Å)	30–2.3 (2.44–2.30)
No. of observations	274926
No. of unique reflections	42000
$< I/\sigma (I) >$ (outermost shell)[a]	10.5 (2.1)
B-factor (Wilson plot) (Å^2)	31.6
Completeness (outermost shell) (%)	95.5 (75.9)
R_{merge} (outermost shell)[b]	0.096 (0.439)
Multiplicity (outermost shell)	6.5 (2.1)
Refinement statistics	
Resolution (outermost shell) (Å)	29.3–2.3 (2.44–2.30)
No. of reflections used (free)	41950 (5131)
Residues included	12–252, 261–314, 324–837
No. of protein atoms	6581
No. of solvent molecules	286
No. of ligand atoms	15 (PLP), 48 (E226: 2 molecules)
R_{cryst}(outermost shell)[c]	0.182 (0.285)
R_{free}(outermost shell)[d]	0.214 (0.339)
r.m.s. deviation of ideality in bond lengths (Å)	0.006
r.m.s. deviation of ideality in bond angles (°)	1.2
r.m.s. deviation of ideality in dihedral angles (°)	22.0
r.m.s. deviation of ideality in improper angles (°)	0.82
Average B (Å^2) for residues	12–252, 261–314, 324–837
Overall	37.6
CA, C, N, O	37.5
Side chain	40.6
Average B (Å^2) for ligands	
PLP	28.8
E226 (orientations I/II)	50.9/36.6
Average B (Å^2) for water molecules	43.2

[a] σ(I) is the standard deviation of I. [b] $R_{merge} = \Sigma_i\Sigma_h | < I_h > - I_{ih}|/\Sigma_i \Sigma_h I_{ih}$, where $< I_h >$ and I_{ih} are the mean and the ith measurements of intensity for reflection h, respectively. [c] $R_{cryst} = \Sigma| |F_o| - |F_c| |/\Sigma|F_o|$, where $|F_o|$ and $|F_c|$ are the observed and calculated structure factor amplitudes, respectively. [d] R_{free} is the corresponding R-value for a randomly chosen 5% of the reflections that were not included in the refinement.

Results and discussion

Synergistic inhibition by E226 and glucose

Kinetic experiments with GPb showed that E226 is an inhibitor of GPb with a $K_i = 13.8$ μM measured in the direction of glycogen synthesis, and in the presence of saturated concentrations of glycogen (1% w/v), AMP (1 mM), and various concentrations of Glc1-P and E226 (Fig. 1A). Measurements of the kinetic parameters of GPb at various E226 and glucose concentrations and fixed concentrations of the substrates Glc1-P (10 mM), AMP (1 mM) and glycogen (1% w/v) indicated that E226 exhibits synergistic inhibition with glucose (with an interaction constant of $\alpha = 0.98 \pm 0.06$ suggesting that both E226 and glucose are able to bind to the enzyme at the same time (Fig. 1B) [31,32]. E226 was also shown to inhibit GPa activity in a manner similar to that of the b form, when assayed in the presence of saturated concentration of glycogen (1% w/v) and varied concentrations of the substrate Glc1-P (3–20 mM) and inhibitor (30–80 μM) in the absence of AMP. The apparent kinetic parameters determined in this case were $K_m = 2.3 \pm 0.2$ mM, $k_{cat} = 56.1 \pm 0.5$ IU·mg^{-1}, and $K_i = 57.8 \pm 7.1$ μM, as expected for the binding of a T-state inhibitor to GPa which is predominantly R-state. Experiments to explore the effects of E226 on glycogen metabolism under physiological conditions (inhibition of glycogenolysis in cell-free liver extracts and in intact hepatocytes) are in progress and the results will be presented elsewhere.

E226 binding to the inhibitor site of GPb

Although the inhibitor site has not yet been used to design inhibitors targeted for therapy of type 2 diabetes mellitus due to its low specificity, its properties have been studied extensively in the liver [33] and in the muscle enzyme (reviewed in [3]). The inhibitor site is located on the surface of the enzyme, between domains 1 (residues 13–484) and 2 (residues 485–842) of the enzyme subunit, some 12 Å from the catalytic site. In the T state, the site obstructs the entrance to the catalytic site tunnel (Fig. 2). In addition,

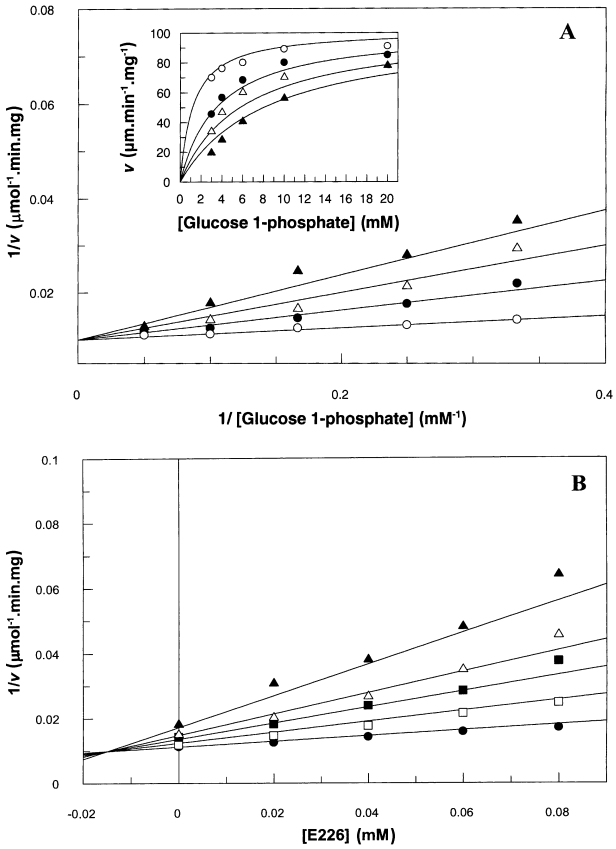

Fig. 1. Inhibition of GPb. (A) Kinetics of E226 inhibition of GPb with respect to Glc1-P. Double reciprocal plot of initial reaction velocity vs. [Glc1/P] at constant concentrations of AMP (1 mM) and glycogen (1% w/v) and various concentrations of E226. Inhibitor concentrations were as follows: 0 µM (○), 20 µM (●), 40 µM (△), 60 µM (▲). Best-fit lines were computer generated according to the equation for competitive inhibition by fitting all of the data at once. The apparent kinetic parameters determined by this method are as follows: K_m = 1.3 ± 0.2 mM, k_{cat} = 100.0 ± 2.6 IU·mg^{-1}, K_i = 13.8 ± 0.2 µM. Inset: fit of the calculated lines to the initial rate measurements. (B) Synergistic inhibition of GPb by E226 and glucose. Dixon plot of reciprocal velocity vs. E226 concentrations at constant concentrations of Glc1-P (10 mM), AMP (1 mM) and glycogen (1% w/v) and various concentrations of glucose. Glucose concentrations were as follows: 0 mM (●), 2 mM (□), 4 mM (■), 6 mM (△), 10 mM (▲). The intersection point above the horizontal axis, corresponding to the dissociation constant of E226 in the presence of glucose with αK_i = 0.0135 mM. Considering that K_i equals 13.8 ± 0.2 µM in the absence of glucose, the interaction constant α between E226 and glucose is 0.98 ± 0.06.

Fig. 2. A schematic diagram of the GPb dimeric molecule viewed down the molecular dyad. One subunit is coloured light green and the other cyan. The positions are shown for the catalytic and the inhibitor site. The catalytic site, marked by glucose (GLC) shown in red and in ball-and-stick representation, is buried at the centre of the subunit accessible to the bulk solvent through a 15-Å long channel. Glucose, a competitive inhibitor of the enzyme that also promotes the less active T state through stabilization of the closed position of the 280 s loop (shown in yellow), binds at this site. The inhibitor site, marked by E226 (shown in mauve), is situated on the surface of the enzyme some 12 Å from the catalytic site and, in the T state, obstructs the entrance to the catalytic site tunnel.

there is no access for the substrate (glycogen) to the catalytic site; access to this site is partly blocked by the 280 s loop (residues 282–287). Glucose, a competitive inhibitor of the enzyme that promotes the T state through localization of the closed position of the 280 s loop, binds at this site. In the T state, Phe285, from the 280 s loop, is stacked close to Tyr613, from the start of the α19 helix (residues 613–631) and together these two hydrophobic aromatic residues form the inhibitor site. Purines, nucleosides, nucleotides and heterocyclic compounds such as flavin mono-nucleotide, flavin-adenine dinucleotide, riboflavin and flavopiridol have been shown to bind at this site in both muscle and liver GPb and GPa [12,31,33–36]). The affinity of these ligands is mainly due to the π–π stacking interactions developed from intercalation of their aromatic rings between the side chains of Phe285 and Tyr613. This intercalation stabilizes the closed position of 280 s loop and promotes the inactive T state. This, in turn, accounts for synergistic inhibition observed when a purine site inhibitor and glucose are both present. On transition from T state to R state, the 280 s loop becomes disordered and displaced, thus opening a channel that allows a crucial arginine, Arg569, to enter the catalytic site in the place previously occupied by Asp283 and create the phosphate recognition site; that also provides access for glycogen substrate to reach the catalytic site [4]. Whether the inhibitor site has a physiological role has yet to be

established but it may be used by an unidentified inhibitor to enhance the effects of the control of liver GPa by glucose, possibly in response to insulin [37,38].

The refined sigmaA weighted F_o–F_c and $2F_o$–F_c electron density maps clearly indicated strong binding of E226 at the inhibitor site, consistent with the kinetic results (Fig. 3A,B). The structural results suggest that the inhibitor site can accommodate two possible orientations of E226, I and II, related by a rotation of $\approx 180°$ around the short axis of the E226 molecule. Each model was fitted in the density map and both orientations were explored in refinement; the best fitting in the electron density map was achieved with orientation I (Fig. 3A). In both orientations, E226 makes similar interactions with the residues of the inhibitor site (Tables 2 and 3). Hence, only orientation I will be considered throughout the discussion.

E226 binds at the inhibitor site with the two indole groups in the same plane and the carbonyl groups at *trans* position with respect to the double bond that connects the two indole moieties (Scheme 1). The most characteristic feature of the E226 binding to GPb is the π-π stacking interactions of the E226 aromatic rings with the aromatic side chains of residues Phe285 and Tyr613 which appear to promote E226 binding (Fig. 3C). There is a hydrogen bond between atom N1 of E226 and Oδ1 of Asn282. Additionally, E226 is involved in a water-mediated network of interactions with GPb residues Asp283, Glu287, Ile570, Ala610, and Met615 (Table 2). The sulphonate group projects into solvent and is not involved in any hydrogen bonding interactions (Fig. 3D). E226, on binding to the enzyme, makes a total of 62 Van der Waals' interactions (48 nonpolar/nonpolar and 14 nonpolar/polar) with GPb residues (Table 3).

On forming the complex with the protein, E226 becomes buried. The solvent accessibilities of the free and bound E226 molecules are 495 $Å^2$ and 182 $Å^2$, indicating that a surface area of 313 $Å^2$ becomes inaccessible to water or that E226 becomes 63% buried in the enzyme complex. The greatest contribution comes from the nonpolar groups, which contribute 251 $Å^2$ (80%) of the surface that becomes inaccessible. On the protein surface, a total of 267 $Å^2$ solvent-accessible surface area becomes inaccessible on binding of E226. The total buried surface area (protein plus ligand) for the GPb/E226 complex is 580 $Å^2$.

The binding of E226 to GPb does not promote any significant changes in the conformation of the polypeptide chain. The superposition of the structures of the native T state GPb and the GPb/E226 complex over well defined residues (12–252, 261–314, 324–837) gave an r.m.s. deviation of 0.158 Å for Cα atoms, indicating that the GPb/E226 structure is similar to that of the native enzyme. There is a small shift in the side chain conformation of Phe285 (0.3–0.5 Å) (Fig. 4A). This residue shifts to optimize van der Waals' interactions with the indole ring. In the native structure there are two water molecules, which are not observed in GPb/E226 structure. These water molecules are displaced by E226 when it binds at the inhibitor site. The interdomain hydrogen-bonding pattern in the vicinity of the inhibitor site, which stabilizes the T state conformation, is retained on binding of E226. E226, on binding to the inhibitor site, inhibits the enzyme through localization of the 280 s loop in its closed, inactive conformation. This prevents the crucial conformational changes that are critical for catalytic activity, e.g. movement of Arg569 into the catalytic site to create the phosphate recognition site, and also prevents the binding of glycogen substrate.

Comparison with caffeine binding

Caffeine, like E226, binds at the inhibitor site of GPb with $K_i \approx 0.1$–0.2 mM and functions with glucose in a synergistic mode [12,31,32]. E226 and caffeine bind in similar places within the inhibitor site. Upon binding, the six-membered ring of caffeine molecule superimposes onto the five-membered ring of E226 indole moiety, which does not have the sulphonate group and these two rings superimpose with an angle of $\approx 8°$. The five-membered ring of caffeine does not superimpose with any of the E226 rings. Indeed, it is placed in the space between the two indole groups of E226 (Fig. 4B). Caffeine, on binding to the hydrophobic pocket of the inhibitor site, is involved in water-mediated interactions with Glu382 and Asp283 and forms 79 van der Waals' contacts (44 nonpolar/nonpolar, four polar/polar, and 39 polar/nonpolar) with GPb residues, while the total buried surface area (protein plus ligand) for the GPb/caffeine complex is 467 $Å^2$ [12]. The r.m.s. deviation between the structures of the GPb/E226 complex and the GPb–caffeine–IMP complex is of 0.164 Å for Cα atoms. There are only minor differences between the two complex structures. The minor conformational changes between the two complex structures, at the inhibitor site, concern small shifts (0.2–0.3 Å) of the side chain atoms of residues Phe285 and Tyr613 (Fig. 4B). Thus, Phe285 and Tyr613 tilt their side chains from their positions in the GPb/caffeine complex by $\approx 8°$ to place the aromatic groups parallel to the E226 plane, adopting a conformation similar to that of the unliganded enzyme.

Caffeine exhibits approximately 10-fold weaker affinity for GPb than E226. The higher potency of E226 could be attributed to a specific hydrogen bond of E226 to Asn282. In the GPb–caffeine complex there are no specific hydrogen bonds apart from those to water molecules. Although caffeine is entirely buried at the inhibitor site, both inhibitors participate in almost the same number of van der Waals' interactions with GPb. E226 is not entirely buried at the inhibitor site but the sulphonate moiety is exposed to the bulk solvent precluding its participation in any direct contacts with the protein.

Comparison with flavopiridol binding

Similarly to caffeine, flavopiridol binds at the inhibitor site of GPb with an IC_{50} of 1 μM [11] and exhibits synergistic inhibition with glucose [12]. It is intercalated between the two aromatic residues Phe285 and Tyr613 and its ring system forms several contacts with GPb, by exploiting a few polar/polar and numerous van der Waals' interactions; it makes a total of four hydrogen bonds to water molecules and 107 van der Waals' interactions (58 nonpolar/nonpolar, six polar/polar, and 43 polar/nonpolar) [12]. The more extensive interactions with the inhibitor site may be one of the reasons that flavopiridol maintains a high affinity. The total buried surface area (protein plus ligand) for the GPb–flavopiridol complex is 618 $Å^2$.

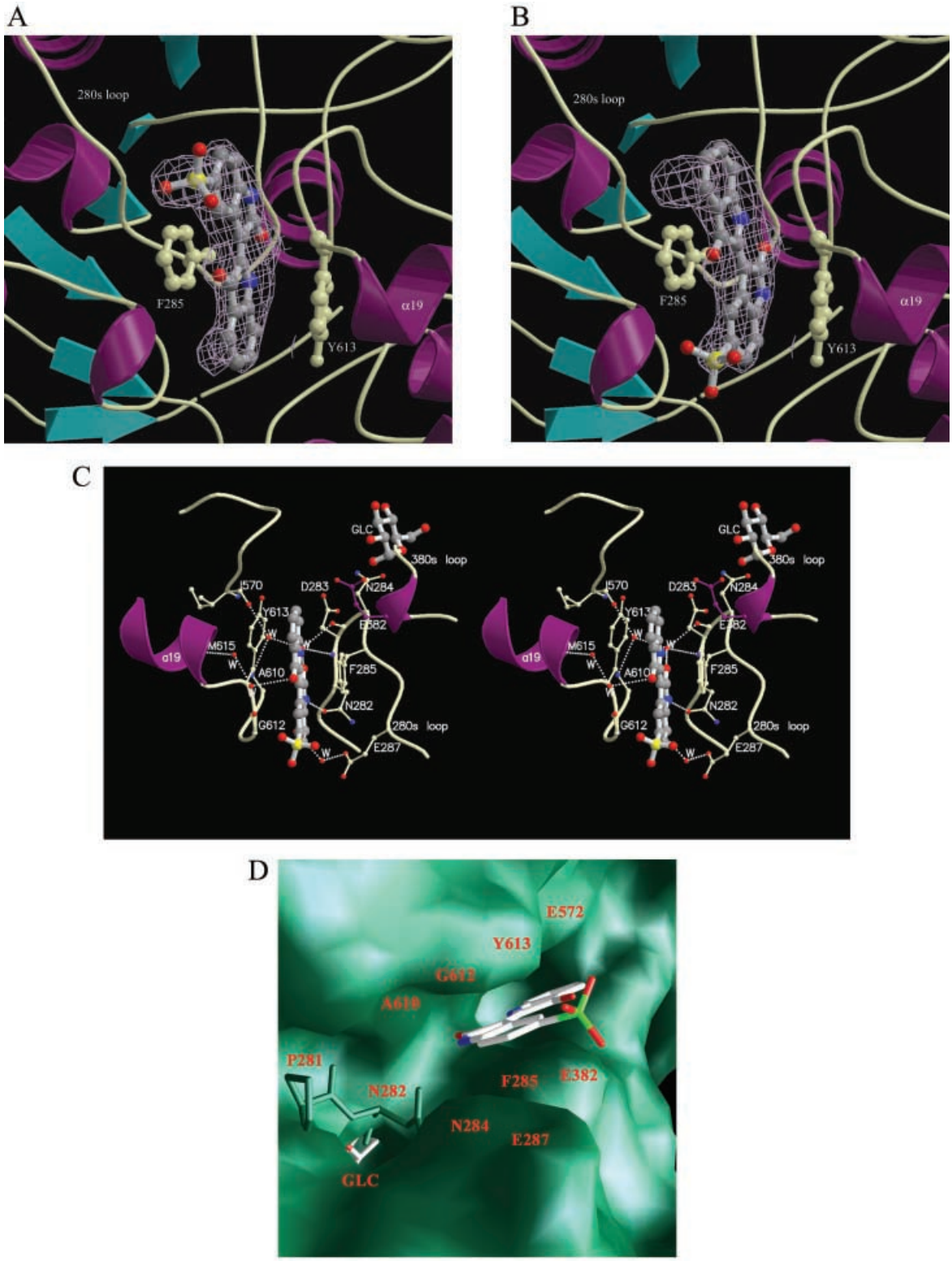

Fig. 3. Binding of E226 to GPb. (A) Diagram of the SigmaA-weighted $2F_o$-F_c electron density map (before incorporating the ligand) showing the stacking of the molecule with Phe285 and Tyr613 at the inhibitor site. The electron density map was calculated using the standard protocol as implemented in CNS v1.1 [23] from the GPb model before incorporating the coordinates of E226 (orientation I). The map is contoured at 1.0 σ level. (B) As in (A) with the E226 in orientation II. (C) Contacts between E226 (orientation I) and GPb, in the vicinity of the inhibitor site shown in stereo. (D) The molecular surface of GPb showing the binding of E226 (orientation I) at the inhibitor site. The residues involved in interactions with the ligand are indicated on the surface. The location of the catalytic site where the glucose molecule binds at the catalytic site of the enzyme is also shown. The figure was prepared using the program GRASP [43].

Table 2. Hydrogen bonds between E226 and residues of the inhibitor site of GPb. Atom names are as in Fig. 1. Wat127 is hydrogen-bonded to Asn282 Oδ1 and to Glu287 Oε2 through another water molecule (Wat126). Wat225 is hydrogen bonded to Asp283 N, Asp283 O, and to another water molecule (Wat224). Wat224 is in turn hydrogen bonded to Ile570 O and to Ala610 N. Wat286 is hydrogen-bonded to Met615 N through another water molecule (Wat233). Hydrogen bond interactions were calculated with the program HBPLUS [42].

		Distance (Å)	
Inhibitor atom	Protein atom	Orientation I	Orientation II
N1	Asn282 Oδ1	2.6	–
N1	Wat127	3.2	–
O2	Wat225	2.9	2.7
O3′	Wat286	3.2	3.4
O51	Wat227	–	3.2

The binding mode of E226 is different from that of flavopiridol (Fig. 4C). Upon binding, the E226 indole moiety, which does not have the sulphonate group, forms an angle of about 30° with the benzopyran-4 one of flavopiridol. The overall structures of both complexes are similar. The r.m.s. deviation between the structures of the GPb–E226 complex and the GPb–flavopiridol complex is 0.159 Å for the Cα atoms. Minor differences between the two structures at the inhibitor site include small shifts of the side chains of Phe285 and Glu382. These differences are also observed when comparing the structures of the unliganded GPb and the GPb–flavopiridol complex. The conformations of Phe285 and Glu382 in the GPb–E226 complex structure are very close to those of the native enzyme.

The superposition of the GPb–E226 structure onto the GPb–flavopiridol structure complex reveals several significant differences. There is an adjacent pocket lined by His571 and Glu572, Arg770 and Phe771, Leu380 and Glu382, Tyr613, and Asn284 of the 280 s loop that can accommodate the chlorophenyl ring of flavopiridol. This part of the ligand exploits 29 van der Waals' contacts dominated by the substantial contacts made to almost all atoms of Glu382 [12]. In contrast, E226 makes no interactions with this pocket. This might indicate that a bulky group present in E226 may confer selectivity and tight binding to GPb.

Comparison to E226 binding to pCDK2–cyclin A complex

The complex structures of the monomeric CDK2–E226 and the pCDK2–cyclin A–E226 have been previously determined at 1.9 Å and 2.5 Å resolution, respectively [13,14]. E226 binds to pCDK2–cyclin A complex more tightly than it binds to GPb. The structure of the complex of E226 with the fully active pCDK2–cyclin A protein complex (PDB code 1E9H) was used for the structural comparison. The crystal structure of the active pCDK2–cyclin A in complex with E226 has shown that E226 binds at the ATP binding site (Fig. 5), which is located between the N- and C-terminal domains. The high potency of this compound derives from its complementarity to the pCDK2–cyclin A binding site, in both shape and chemical character. The inhibitor forms three hydrogen bonds with the protein main chain atoms at

Table 3. Van der Waals' contacts between E226 and residues of the inhibitor site of GPb. Van der Waals' distances are calculated using van der Waals' contact radii for atoms: C, 2.05 Å; O, 1.54 Å; and N, 1.7 Å.

Inhibitor atom	Protein atom (Orientation I)	No of contacts	Protein atom (Orientation II)	No of contacts
C2′	Phe285, Cγ, Cδ1, Cδ2, Cε1, Cε2, Cζ; Tyr613 Cγ	7	Phe285, Cγ, Cδ1, Cδ2, Cε1, Cε2, Cζ	6
C3′	Phe285 Cδ1, Cε1, Cζ	3	Phe285 Cδ2, Cε1, Cε2, Cζ	4
O3′	–	–	Phe285 Cζ	1
C6′	Tyr613 Cε2, Cζ, Oη	3	Glu287 Cδ; Gly612 Cα	2
C7′	Tyr613 Cε1, Cε2, Cζ, Oη	4	Asn282 Oδ1; Gly612 Cα	2
C8′	Phe285 Cδ1, Cε1; Tyr613 Cγ, Cε1, Cδ2, Cε2, Cζ	7	Phe285 Cδ2, Cε2; Gly612 Cα, C	4
C9′	Phe285 Cδ1, Cε1; Tyr613 Cε2	3	Phe285 Cε2; Gly612 C, O	3
N1′	Phe285 Cγ, Cδ1; Tyr613 Cγ	3	Phe285 Cδ2, Cε2	2
C2	Asn282 Oδ1; Phe285 Cβ, Cγ, Cδ2; Ala610 Cβ; Tyr613 Cβ	6	Phe285 Cβ, Cγ, Cδ1; Tyr613, Cβ, Cγ, Cδ1, Cε1	7
O2	Phe285 Cβ, Cγ; Ala610 Cβ	3	Phe285 Cβ, Cγ	2
C3	Phe285 Cγ, Cδ1, Cδ2, Cε2, Cζ; Tyr613 Cα, Cβ	7	Phe285 Cγ, Cδ1, Cδ2, Cε1, Cε2, Cζ; Tyr613 Cβ, Cγ, Cδ2	9
C4	Phe285 Cε2; Gly612 C, O	3	Phe285 Cε1	1
C6	Gly612 Cα	1	Tyr613 Cε2, Cζ	2
C7	Gly612 Cα, C	2	Tyr613 Cε1, Cε2, Cζ, Oη	4
C8	Asn282 Oδ1; Phe285 Cδ2; Gly612 Cα, CCε1, Cδ2, Cε2, Cζ	4	Phe285 Cδ1; Tyr613 Cγ, Cδ1,	7
C9	Phe285 Cδ2, Cε2; Gly612 C, O	4	Phe285 Cδ1, Cε1; Tyr613 Cγ, Cδ2, Cε2	5
N1	Asn282 Cγ; Ala610 Cβ	2	Tyr613 Cγ, Cδ1, Cε1, Cζ	4
Total	Five residues	62	Four residues	65

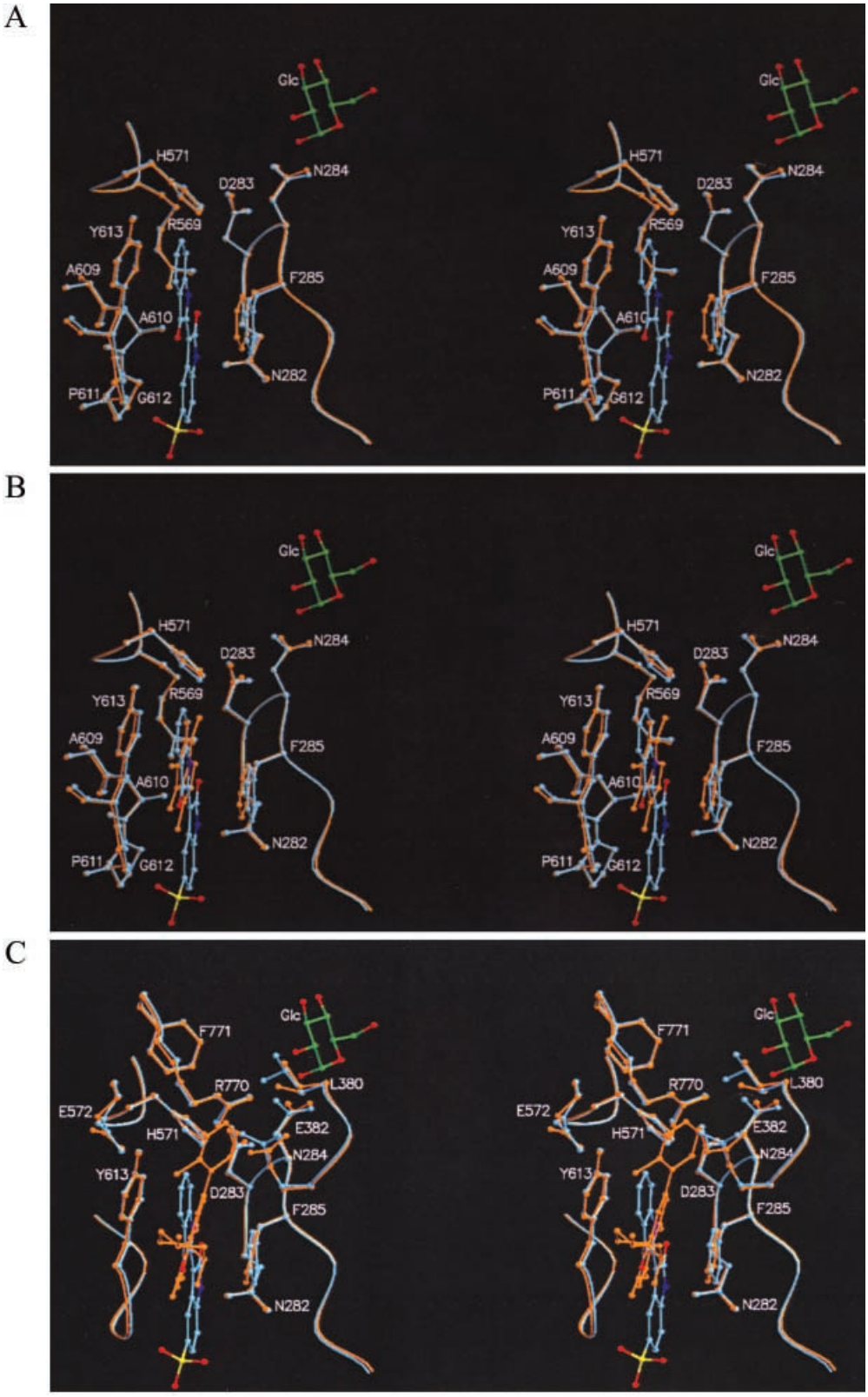

Fig. 4. Structural comparison of GPb–E226, GPb–caffeine, and GPb–flavopiridol complexes. Superimposed structures of (A) GPb–E226 complex onto the native GPb, (B) GPb–E226 complex onto the GPb–caffeine complex, and (C) GPb–E226 complex onto the GPb–flavopiridol complex. GPb–E226 complex is shown in cyan. Native GPb, GPb–caffeine complex, and GPb–flavopiridol complex are shown in orange. The catalytic site is marked by glucose (shown in green).

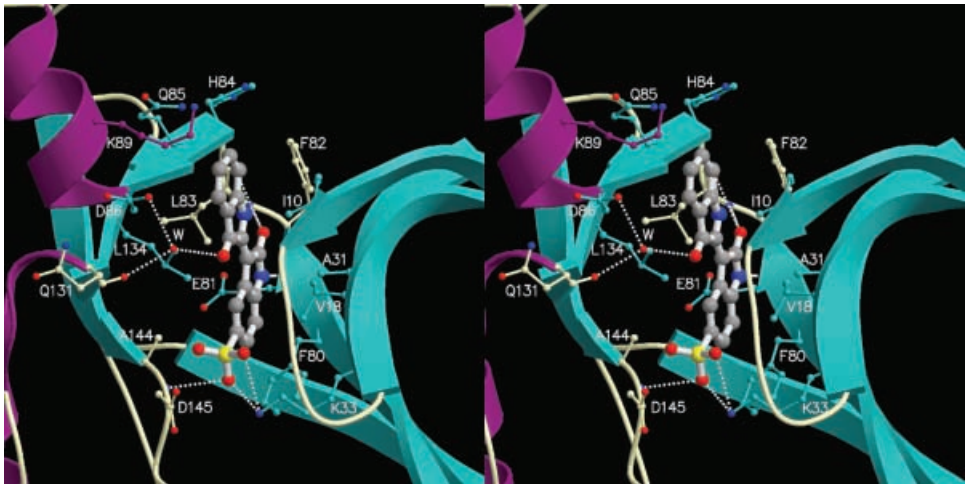

Fig. 5. Binding of E226 to pCDK2–cyclin A. Stereodiagram showing the contacts between E226 and pCDK2–cyclin A (pdb code 1E9H [14]).

the hinge region. The N1 and O2 atoms of E226 are hydrogen bonded with the main chain oxygen of Glu81 and the NH group of Leu83 resembling interactions observed in the complexes between monomeric CDK2 and the ligands ATP and staurosporine [39]. Atom N1 of E226 forms a third hydrogen bond with the main chain oxygen of Leu83. The plane of indole rings packs against hydrophobic residues Val18, Ala31 and Leu134, which constitute the surface offered by the N- and C-terminal domains of CDK2 to the binding cleft. Atoms C6 and C7 of E226 form an edge-to-face aromatic contact with Phe80 and the C4′–C9′ ring extends out of the pocket to contact a tunnel of hydrophobic residues constituted by Phe82, Ile10 and the alkyl portion of Lys89 [14]. Other key interactions occur between the sulphonate group with Lys33 and the DFG segment of CDK2. More specifically, Lys33 bridges two of the sulphonate oxygen atoms, while another oxygen atom makes a hydrogen bond with the main-chain N of Asp145. In contrast, the presence of the sulphonate group does not confer significantly to the binding of E226 to GSK-3β ($IC_{50} = 280$ nM [40]). Upon binding to CDK2, a surface of 453 Å^2 (250 Å^2 nonpolar) of ligand and 260 Å^2 (184 Å^2 nonpolar) of protein become inaccessible to solvent [14]. Thus, the total buried surface area (ligand + protein) is 713 Å^2. Affinities calculated by LUDI [14] for the interaction of E226 with monomeric or pCDK2/cyclin A differ by a factor of approximately 10 in the predicted K_d.

Comparison between pCDK2–cyclin A–E226 and GPb–E226 complex structures show that E226 forms different interactions with the two proteins. Because of its high complementarity to pCDK2–cyclin A, E226 exploits specific hydrogen bonds that mimic those of ATP and nonpolar interactions that are made mostly to aliphatic chains. Additionally, the sulphonate group is involved in hydrogen bonding interactions. In GPb–E226 there are no specific direct hydrogen bonds to the protein apart to that with Asn282, the sulphonate group makes no interactions with the protein, while the nonpolar interactions involve mainly π-π stacking interactions with the aromatic groups of Phe285 and Tyr613. This may explain why E226 is a more potent inhibitor of pCDK2–cyclin A complex than of GPb.

Conclusion

In this study, we have determined the binding mode of E226 to GPb and compared GPb–E226 complex structure with GPb–caffeine and GPb–flavopiridol structures. Our structures provide a clear picture of the binding modes of these ligands in the inhibitor site of GPb. Flavopiridol is a more potent inhibitor of GPb than E226 (E226 exhibits 14-fold lower affinity to the enzyme). Our crystallographic experiments rationalize this difference by showing how E226 and flavopiridol are positioned at the inhibitor site. The extended ring system of flavopiridol forms more hydrophobic interactions with the protein than E226, leading to better affinity for GPb. E226–flavopiridol comparison has identified a pocket occupied by the chlorophenyl ring of flavopiridol. The chlorophenyl ring pocket may represent a good template for the design of specific and tight synthetic inhibitors. The inhibitor site is identically conserved in all mammalian GPs [41], indicating that E226 is likely to inhibit also liver GP, the more important target enzyme in terms of treatment of type 2 diabetes, and brain GP, the species present in proliferating cells [9]. We have also compared the interactions between E226 with the active pCDK2–cyclin A complex and GPb. The structural comparison of GPb–E226 complex with CDK2–cyclin A–E226 complex structure shows that E226 makes different interactions with two nonhomologous enzymes and illustrates how two different enzymes use different parts of an inhibitor to provide specificity.

Acknowledgements

This work was supported by the General Secretariat of Research and Technology of the Greek Ministry of Development (PENED-204/2001), ENTER (01-EP6), a Royal Society Joint Project (to L.N. Johnson and NGO), AstraZeneca, Macclesfield, UK, EMBL Hamburg Outstation through the IHPP (HPRI-CT-1999-00017), SRS Daresbury Laboratory through the (IHPP HPRI-CT-1999-00012), and EU contract HPRI-CT-1999-00097 for work at CDSB, Jena, Germany, through minor grants to NGO. We also thank Drs K.E. Tsitsanou, S.E. Zographos, and V.T. Skamnaki for their initial contributions to the project.

References

1. McCormack, J.G., Westergaard, N., Kristiansen, M., Brand, C.L. & Lau, J. (2001) Pharmacological approaches to inhibit endogenous glucose production as a means of anti-diabetic therapy. *Curr. Pharm. Des.* **7**, 1451–1474.
2. Treadway, J.L., Mendys, P. & Hoover, D.J. (2001) Glycogen phosphorylase inhibitors for treatment of type 2 diabetes mellitus. *Expert. Opin. Invest. Drugs* **10**, 439–454.
3. Oikonomakos, N.G. (2002) Glycogen phosphorylase as a molecular target for type 2 diabetes therapy. *Curr. Protein Pept. Sci.* **3**, 561–586.
4. Johnson, L.N. (1992) Glycogen phosphorylase: control by phosphorylation and allosteric effectors. *FASEB J.* **6**, 2274–2282.
5. Oikonomakos, N.G., Acharya, K.R. & Johnson, L.N. (1992) Rabbit muscle glycogen phosphorylase b: structural basis of activation and atalysis. In *Post-Translational Modification of Proteins* (Harding, J.J. & Crabbe, M.J.C., eds), pp. 81–151. CRC Press, Boca Raton, FL.
6. Alemany, S. & Cohen, P. (1986) Phosphorylase a is an allosteric inhibitor of the glycogen and microsomal form of rat hepatic protein phosphatase 1. *FEBS Lett.* **198**, 194–202.
7. Newgard, C.B., Hwang, P.K. & Fletterick, R.J. (1989) The family of glycogen phosphorylases: structure and function. *Crit. Rev. Biochem. Mol. Biol.* **24**, 69–99.
8. Bollen, M. & Stalmans, W. (1992) The structure, role and regulation of Type I protein phosphatases. *Crit. Rev. Biochem. Mol. Biol.* **27**, 227–281.
9. Schnier, J.B., Nishi, K., Monks, A., Gorin, F.A. & Bradbury, E.M. (2003) Inhibition of glycogen phosphorylase (GP) by CP-91,149 induces growth inhibition correlating with brain GP expression. *Biochem. Biophys. Res. Commun.* **309**, 126–134.
10. McLaughlin, F., Finn, P. & La Thangue, N.B. (2003) The cell cycle, chromatin and cancer: mechanism-based therapeutics come of age. *Drug Discov. Today* **8**, 793–802.
11. Kaiser, A., Nishi, K., Gorin, F.A., Walsh, D.A., Bradbury, E.M. & Schnier, J.B. (2001) The cyclin-dependent kinase (CDK) inhibitor flavopiridol inhibits glycogen phosphorylase. *Arch. Biochem. Biophys.* **386**, 179–187.
12. Oikonomakos, N.G., Schnier, J.B., Zographos, S.E., Skamnaki, V.T., Tsitsanou, K.E. & Johnson, L.N. (2000) Flavopiridol inhibits glycogen phosphorylase by binding at the inhibitor site. *J. Biol. Chem.* **275**, 34566–34573.
13. Hoessel, R., Leclerc, S., Endicott, J.A., Nobel, M.E., Lawrie, A., Tunnah, P., Leost, M., Damiens, E., Marie, D., Marko, D., Niederberger, E., Tang, W., Eisenbrand, G. & Meijer, L. (1999) Indirubin, the active constituent of a Chinese antileukaemia medicine, inhibits cyclin-dependent kinases. *Nat. Cell Biol.* **1**, 60–67.
14. Davies, T.G., Tunnah, P., Meijer, L., Marko, D., Eisenbrand, G., Endicott, J.A. & Noble, M.E. (2001) Inhibitor binding to active and inactive CDK2: the crystal structure of CDK2-cyclin A/indirubin-5-sulphonate. *Structure* **9**, 389–397.
15. Leclerc, S., Garnier, M., Hoessel, E., Marko, D., Bibb, J.A., Snyder, G.L., Greengard, P., Biernat, J., Wu, Y.Z., Mandelow, E.M., Eisenbrand, G. & Meijer, L. (2001) Indirubins inhibit glycogen synthase-3 beta and CDK5/p25, two protein kinases involved in abnormal tau phosphorylation in Alzheimer's disease. A property common to most cyclin-dependent kinase inhibitors? *J. Biol. Chem.* **276**, 251–260.
16. Meijer, L., Skaltsounis, A.-L., Magiatis, P., Polychronopoulos, P., Knockaert, M., Leost, M., Ryan, X.P., Vonica, C.A., Brivanlou, A., Dajani, R., Crovace, C., Tarricone, C., Musacchio, A., Roe, S.M., Pearl, L. & Greengard, P. (2003) GSK-3-Selective inhibitors derived from Tyrian purple indirubins. *Chem. Biol.* **10**, 1255–1266.
17. Polychronopoulos, P., Magiatis, P., Skaltsounis, A.-L., Myrianthopoulos, V., Mikros, E., Tarricone, A., Musacchio, A., Roe, S.M., Pearl, L., Leost, M., Greengard, P. & Meijer, L. (2004) Structural basis for the synthesis of indirubins as potent and selective inhibitors of glycogen synthase kinase-3 and cyclin-dependent kinases. *J. Med. Chem.* **47**, 935–946.
18. Oikonomakos, N.G., Kontou, M., Zographos, S.E., Watson, K.A., Johnson, L.N., Bichard, C.J., Fleet, G.W. & Acharya, K.R. (1995) N-acetyl-beta-D-glucopyranosylamine: a potent T-state inhibitor of glycogen phosphorylase. A comparison with alpha-D-glucose. *Protein Sci.* **4**, 2469–2477.
19. Oikonomakos, N.G., Tsitsanou, K.E., Zographos, S.E., Skamnaki, V.T., Goldmann, S. & Bischoff, H. (1999) Allosteric inhibition of glycogen phosphorylase a by the potential antidiabetic drug 3-isopropyl 4-(2-chlorophenyl) -1,4-dihydro-1-ethyl-2-methyl-pyridine-3,5,6-tricarboxylate. *Protein Sci.* **8**, 1930–1945.
20. Helmreich, E.J.M. & Cori, C.F. (1964) The role of adenylic acid in the activity of phosphorylase. *Proc. Natl Acad. Sci. USA* **51**, 131–138.
21. Otwinowski, Z. & Minor, W. (1997) Processing of X-ray diffraction data collected in oscillation mode. *Methods Enzymol.* **276**, 307–326.
22. French, S. & Wilson, K.S. (1978) On the treatment of the negative intensity observations. *Acta Crystallogr.* **A34**, 517–525.
23. Brünger, A.T., Adams, P.D., Clore, G.M., DeLano, W.L., Gros, P., GrosseKunstleve, R.W., Jiang, J.S., Kuszewski, J., Nilges, M., Pannu, N.S., Read, R.J., Rice, L.M., Simonson, T. & Warren, G.L. (1998) Crystallography & NMR system: a new software suite for macromolecular structure determination. *Acta Crystallogr.* **D54**, 905–921.
24. Jones, T.A., Zou, J.Y., Cowan, S.W. & Kjeldgaard, M. (1991) Improved methods for building models in electron density maps & the location of errors in these models. *Acta Crystallogr. A* **47**, 110–119.
25. Laskowski, R.A., MacArthur, M.W., Moss, D.S. & Thornton, J.M. (1993) PROCHECK – A program to check the stereochemical quality of protein structures. *J. Appl. Crystallogr.* **26**, 283–291.
26. CCP4 (1994) The CCP4 suite. Programs for Protein Crystallography. *Acta Crystallogr. D* **50**, 760–763.
27. Read, J. (1986) Improved Fourier coefficient for maps using phases from partial structures with errors. *Acta Crystallogr. A* **42**, 140–149.
28. Hubbard, S.J. & Thornton, J.M. (1993) *NACCESS*. Department of Biochemistry and Molecular Biology, University College, London.
29. Kraulis, P.J. (1991) MOLSCRIPT – A program to produce both detailed & schematic plots of protein structures. *J. Appl. Crystallogr.* **24**, 946–950.
30. Merritt, E.A. & Bacon, D.J. (1997) Raster3D: Photorealistic molecular graphics. *Methods Enzymol.* **B277**, 505–524.
31. Kasvinsky, P.J., Shechosky, S. & Fletterick, R.J. (1978) Synergistic regulation of phosphorylase a by glucose and caffeine. *J. Biol. Chem.* **253**, 9102–9106.
32. Madsen, N.B., Shechosky, S. & Fletterick, R.J. (1983) Site–site interactions in glycogen phosphorylase b probed by ligands specific for each site. *Biochemistry* **22**, 4460–4465.
33. Ekstrom, J.L., Pauly, T.A., Carty, M.D., Soeller, W.C., Culp, J., Danley, D.E., Hoover, D.J., Treadway, J.L., Gibbs, E.M., Fletterick, R.J., Day, Y.S., Myszka, D.G. & Rath, V.L. (2002) Structure-activity analysis of the purine binding site of human liver glycogen phosphorylase. *Chem. Biol.* **9**, 915–924.
34. Sprang, S.R., Fletterick, R.J., Stern, M.J., Yang, D., Madsen, N.B. & Sturtevant, J.S. (1982) Analysis of an allosteric binding site: The nucleoside inhibitor site of phosphorylase a. *Biochemistry* **21**, 2036–2048.

35. Tsitsanou, K.E., Skamnaki, V.T. & Oikonomakos, N.G. (2000) Structural basis of the synergistic inhibition of glycogen phosphorylase a by caffeine and a potential antidiabetic drug. *Arch. Biochem. Biophys.* **384**, 245–254.
36. Chebotareva, N., Klinov, S.V. & Kurganov, B.I. (2001) Regulation of muscle glycogen phosphorylase by physiological effectors. *Biotechnol. Genet Eng Rev.* **18**, 265–297.
37. Kasvinsky, P.J., Fletterick, R.J. & Madsen, N.B. (1981) Regulation of the dephosphorylation of glycogen phosphorylase a and synthase b by glucose and caffeine in isolated hepatocytes. *Can. J. Biochem.* **59**, 387–395.
38. Ercan-Fang, N. & Nuttall, F.Q. (1997) The effect of caffeine and caffeine analogs on rat liver phosphorylase a activity. *J. Pharmacol. Exp. Ther.* **280**, 1312–1318.
39. Noble, M.E. & Endicott, J.A. (1999) Chemical inhibitors of cyclin-dependent kinases: insights into design from X-ray crystallographic studies. *Pharmacol. Ther* **82**, 269–278.
40. Bertrand, J.A., Thieffine, S., Vulpetti, A., Cristiani, C., Valsasina, B., Knapp, S., Kalisz, H.M. & Flocco, M. (2003) Structural characterization of the GSK-3β active site using selective and non-selective ATP-mimetic inhibitors. *J. Mol. Biol.* **333**, 393–407.
41. Hudson, J.W., Golding, G.B. & Crerar, M.M. (1993) Evolution of allosteric control in glycogen phosphorylase. *J. Mol. Biol.* **234**, 700–721.
42. McDonald, I.K. & Thornton, J.M. (1994) Satisfying hydrogen bonding potential in proteins. *J. Mol. Biol.* **238**, 777–793.
43. Nicholls, A. & Honig, B. (1991) A rapid finite difference algorithm, utilising successive over relaxation to solve the Poisson-Boltzmann equation. *J. Comput. Chem.* **12**, 435–445.